Preparation of pesticide-loaded microcapsules by liquid-driven coaxial flow focusing for controlled release

Fengjing Zhong, Chaoyu Yang, Qiang Wu, Shiyu Wang, Lei Cheng, Pankaj Dwivedi, Zhiqiang Zhu, Ting Si & Ronald X. Xu

Published online: 08 Jun 2019.

Submit your article to this journal ⬚

View related articles ⬚

View Crossmark data ⬚

Taylor & Francis
Taylor & Francis Group

Check for updates

# Preparation of pesticide-loaded microcapsules by liquid-driven coaxial flow focusing for controlled release

Fengjing Zhong[a]*, Chaoyu Yang[b]*, Qiang Wu[b], Shiyu Wang[b], Lei Cheng[c], Pankaj Dwivedi[b], Zhiqiang Zhu[b], Ting Si[d], and Ronald X. Xu[b,e]

[a]Department of Polymer Science and Engineering, University of Science and Technology of China, Hefei, China; [b]Department of Precision Machinery and Precision Instrumentation, University of Science and Technology of China, Hefei, China; [c]Hospital, University of Science and Technology of China, Hefei, China; [d]Department of Modern Mechanics, University of Science and Technology of China, Hefei, China; [e]Department of Biomedical Engineering, The Ohio State University, Columbus, OH, USA

ABSTRACT

Microencapsulation of pesticide can reduce mammalian toxicity, phyto-toxicity, and protect the pesticides from rapid environmental degradation. The aim of this study was to develop a liquid-driven coaxial flow focusing (LDCFF) process for fabricating pesticide-loaded microcapsules having high encapsulation efficiency, loading efficiency and yield. We have optimized and evaluated the effects of process parameters on the size and morphology of pesticide-loaded microcapsules. The release of pesticides from pesticide-loaded microcapsules has sustained release profiles, which depends on their core-shell structure and shell material degradation process. LDCFF process enables successful encapsulation of pesticides in microcapsules with tunable characteristics important in pesticide applications.

GRAPHICAL ABSTRACT
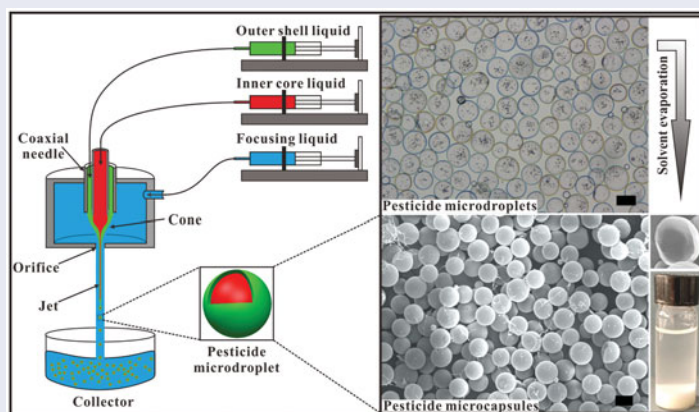
1. Introduction

Pesticides are playing an important role in modern agricultural productions. However, many pesticides would cause environmental pollution in water, soil and atmosphere[1]. Besides, some pesticides like pyraclostrobin are to be sprayed many times because of their instability caused by photolysis, hydrolysis or other factors. Pyraclostrobin is a kind of broad-spectrum fungicide with a pyrazole structure that is photo-unstable. The photolysis half-life of pyraclostrobin in water is 1.7 days[2]. Pyraclostrobin-loaded microcapsules provide a good approach for better efficacy. Therefore, the microencapsulation of pesticide offers a relatively safer type of pesticide delivery system[3,4]. Pesticide microcapsule formulations have many advantages, such as reducing mammalian toxicity, controlling evaporation, reducing phytotoxicity, protecting pesticide from environmental degradation and reducing environmental pollution caused by pesticide[5–8].

To prepare pesticide-loaded microcapsules, some of the most commonly reported methods include interfacial polymerization[9,10], in situ polymerization[11] and complex coacervation[12–14]. Although these methods have their individual advantages, they also have some limitations. In

polymerization process, the applied monomers are highly reactive and the process is usually affected by side reactions. These reactions are also highly sensitive to temperature and pH, leading to difficult controlling of consistent microcapsule formation. Moreover, the complex coacervation method often has relatively complicated process with low encapsulation efficiency.

In recent years, microfluidic technology is being applied in rapid trace detection of residual pesticides[15,16]. Besides, it has already shown superior capabilities in microdroplet or microsphere production, which can also serve as a method to fabricate microcapsules[17]. For example, electrohydrodynamic jetting and electroemulsification methods[18–20] can produce microcapsules with small size and high encapsulation efficiency. Under the influence of an electric field, the fluid undergoes self-repulsion or attraction to form a microcapsule. However, it usually requires a very stable environment to ensure the operating status of the fluid. Glass microcapillaries and PDMS microchannels methods[21–24] can fabricate microcapsules with uniform size and high encapsulation efficiency. However, these methods require a high precision of the device and the production efficiency is often relatively low. Recently, a simple and efficient 3 D coaxial flow focusing method is developed to produce microcapsules[25,26]. Compared with the encapsulation approaches mentioned above, the flow focusing approach is able to produce microcapsules with low cost, high encapsulation rate, high productivity, high consistency in size and good controllability[27,28].

Here, a liquid-driven coaxial flow focusing (LDCFF) process is developed to fabricate pyraclostrobin-loaded poly (lactic-co-glycolic acid) (PLGA) microcapsules. The process produces microcapsules by consecutive steps of double emulsions' formation followed by shell formation during solvent evaporation. It is reported that biodegradable biopolymers are readily available in production, like polyacrylamide[29], ethyl cellulose[30], starch[31], chitosan[32], and PLGA[33]. We have chosen PLGA as a shell material exactly based on its biodegradability. The final in vivo products of PLGA metabolism are lactic acid and glycolic acid, doing no harm to humans and environment, and therefore, PLGA is suitable for the development of safe and green microcapsules. Process parameters can be easily adjusted to control the size and shell thickness of the prepared microcapsules and further to control pyraclostrobin release rates in the PLGA degradation process. The effects of process parameters on the morphology, size, encapsulation efficiency, and controlled release behavior of the microcapsules are systematically investigated, providing valuable information for the rational design of pesticide loaded microcapsules suitable for industrial production and commercial applications.

2. Materials and methods

2.1. Materials

The chemicals and reagents used in our experiments are as follows: Poly(vinyl alcohol) (PVA, Mw: 13000-23000 g/mol, 87-89% hydrolyzed, Sigma-Aldrich, St. Louis, MO),

poly(lactic-co-glycolic acid) (PLGA, Mw: 40000-50000, 80000-100000, 110000-130000 g/mol in trichloromethane of 25 °C, Shandong Institute of Medical Instrument, China), acetonitrile and 99.5% dichloromethane (Sinopharm Chemical Reagent Co., Ltd, China), methyindocarbocyanine perchlorate (97%, Sigma-Aldrich, St. Louis, MO), 50 wt% pyraclostrobin suspension (Yingtaijiahe of Beijing, China). The distilled water is obtained from Nanopure infinity water purification system (Millipore Direct-Q3).

2.2. Methods

2.2.1. Experimental setup for LDCFF process

The schematic diagram of the LDCFF experimental setup, including a stainless steel coaxial needle, three injection pumps, a pressure chamber, and a monitor is shown in Figure 1[28,34]. The coaxial needle is fabricated by laser welding[28,34]. The coaxial needle consists of two needles nested together, of which one has 0.25 mm and 0.51 mm inner and outer diameters while the other has 0.90 mm and 1.20 mm inner and outer diameters, respectively. The coaxial needle with high sealing and concentricity could provide a uniform flow field[35]. The coaxial needle is mounted in the pressure chamber. The outlet of the coaxial needle faces a small orifice with a diameter of 0.3 mm and the vertical distance between them is 1.2 mm. Two syringe pumps (WK-101P, Nanjing Anerke Electronics Technology Co., Ltd, China) provide the continuous flows of inner core liquid and outer shell liquid, and one syringe pump (WK-102P, Nanjing Anerke Electronics Technology Co., Ltd, China) provides continuous flow of focusing liquid. To achieve high productivity by this method, a number of coaxial needles can be easily scaled up and high flow rate pumps can be used directly. A CCD camera (Allied Vision Technologies) equipped with a microscope lens is used to monitor the fluid dynamics in the LDCFF process. A strobe flashlight is used for illumination in real time from the other side of the device. In LDCFF process, a cone-jet structure driven by focusing
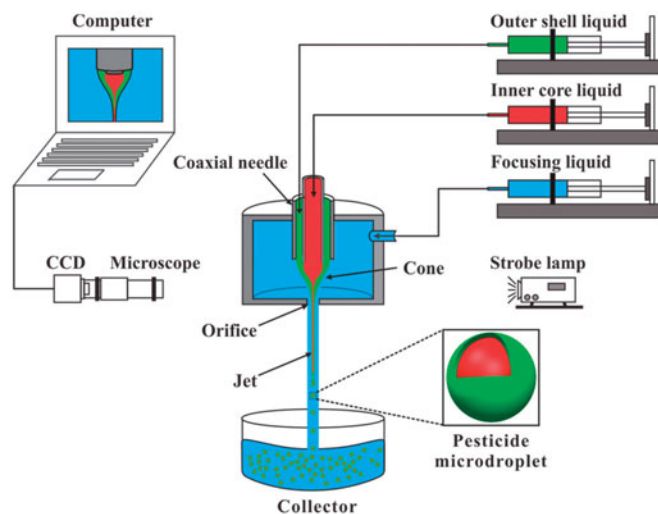

Figure 1. Schematic of the experimental setup for producing microcapsules by the LDCFF process.

liquid in the pressure chamber appears and then passes through the orifice. After that, the jet breaks up into micro-droplets as a result of the perturbation propagation along the jet surface[33–39]. The pesticide suspension is well encapsulated in the oil phase and microcapsules are finally formed after solvent evaporation. This LDCFF assembly is easy to set up, making it available for industrial mass production.

2.2.2. Fabrication of pyraclostrobin-loaded PLGA microcapsules

The pyraclostrobin-loaded PLGA microcapsules are fabricated by LDCFF process as mentioned above. 100 g PVA is dissolved in 1000 mL distilled water to get the 0.1 g/mL PVA aqueous solution. 2 mL 0.1 g/mL PVA aqueous solution, 2 mL 50 wt% pyraclostrobin suspension and 6 mL distilled water are uniformly mixed to be used as the inner core liquid. As for the outer shell liquid, 0.8 g PLGA is dissolved in 10 mL dichloromethane. 100 mL 0.1 g/mL PVA aqueous solution is diluted 10 times to be 0.01 g/mL PVA aqueous solution and used as the focusing liquid. Typically, the flow rates of inner core liquid (Q_i), outer shell liquid (Q_o) and focusing liquid (Q_f) are optimized to be $Q_i = Q_o = 5$ mL/h, $Q_f = 800$ mL/h, respectively. The cone-jet mode can be generated instead of other modes[34] in the vicinity of such parameters. With the perturbation propagating and amplifying, the jet issuing from the orifice breaks into double emulsion microdroplets. After solvent evaporation for 12 h at room temperature, the microcapsules are finally formed. Then the microcapsules are washed three times with distilled water and then dried for 24 h in a vacuum freeze dryer (Songyuan Technology of Beijing, China). Also, PLGA with different molecular weights (40000-50000, 80000-100000 and 1100000-1300000 g/mol) and concentrations (30, 60 and 90 mg/mL) is used to prepare microcapsules. The cone-jet mode could be stable in a wide range of process parameters, so that the flow rates of the three phases can be adjusted to fabricate microcapsules with different sizes and shell thicknesses. Usually, with the increase of Q_f or decrease of Q_i and Q_o, the size of microcapsules would decrease, while the shell thickness would increase with the proportion of Q_i and Q_o decreasing.

2.2.3. Characterization of pyraclostrobin-loaded PLGA microcapsules

The cone-jet configuration and jet breakup process are monitored by the CCD camera. The pyraclostrobin-loaded PLGA microcapsules are characterized by optical microscopy, laser scanning confocal microscopy (methyindocarbocyanine perchlorate is added into the outer shell liquid as fluorescence dye) and scanning electron microscopy (SEM). The size distribution of the PLGA microcapsules is counted and analyzed by Image-Pro Plus software and Origin-Pro 8.0 software. The encapsulation efficiency (EE) should be 100% in theory for that the pyraclostrobin is suspended in inner liquid and it would not leak out of the microdroplets through the outer shell oil phase. During solvent evaporation, a small amount of pyraclostrobin may dissolve in the

oil phase and adhere to the shell. As for the encapsulation efficiency (EE), it can be calculated with the Eq. 1:

$$EE(\%) = \frac{(\text{weight of loaded drugs})/}{(\text{total weight of drugs})} \times 100\% \qquad (1)$$

The specific measurement steps of the actual value of EE are described as follows. Six samples were prepared by the liquid-driven coaxial flow focusing under the same conditions ($Q_i = 10$ mL/h, $Q_o = 5$ mL/h, $Q_f = 800$ mL/h, and the collection time of 1.5 min). After solvent evaporation for 12 h at room temperature, 3 samples were added by appropriate amount of acetonitrile and water solution to 50 mL (acetonitrile and water volume ratio = 1:1) and used for total weight of drugs calculation. Supernatants of the remaining 3 samples were removed after washing and centrifuging. Then the 3 samples were added by appropriate amount of acetonitrile and water solution to 50 mL (acetonitrile and water volume ratio = 1:1) and used for weight of loaded drugs calculation. The supernatants of the 6 samples were taken out to measure the absorption spectrum after sonication and centrifuging. The total weight of drugs and the weight of loaded drugs were calculated to be 594.4 and 558.3 μg based on the standard absorption curve of pyraclostrobin ($y = 0.058x - 0.014$, $R^2 = 0.998$). So the actual value of EE can be calculated to be 93.9% which is very close to the theoretical value.

As for the loading efficiency (LE), it can be calculated with the Eq. 2:

$$LE(\%) = \frac{(\text{weight of loaded drugs})/}{(\text{total weight of the microcapsules})} \times 100\% \qquad (2)$$

Assuming that the EE equals to 100%, the LE can also be calculated using the following Eq. 3:

$$LE(\%) = \frac{C_i Q_i}{C_i Q_i + C_o Q_o} = \frac{Q_i}{Q_i + \frac{C_o}{C_i} Q_o} = \frac{C_i}{C_i + C_o \frac{Q_o}{Q_i}} \qquad (3)$$

where C_i, C_o are the concentrations of the inner and outer phases, Q_i, Q_o are the flow rates of the inner and outer phases, respectively. Given $Q_i = Q_o$, $C_i=0.1$ and $C_o =0.08$, the LE can be calculated to be 55.56%. As the value of C_i or Q_i increases, the LE will increase. Considering suspending agent (there is 3 wt% in 50 wt % pyraclostrobin suspension), the actual value of LE is slightly lower than the calculated value.

2.2.4. Sustained release experiment

The sustained release experiment is designed to compare and simulate the release of different pyraclostrobin-loaded PLGA microcapsules. Dialysis bags (width: 55 mm, Mw: 3500, Sangon Biotech Co., Ltd, China) are put into distilled water for about 20 min. Then 10 mg pyraclostrobin-loaded PLGA microcapsules are dispersed in 5 mL distilled water and transferred into the dialysis bags and sealed. After that, the dialysis bags are immersed in a mixture (300 mL) of acetonitrile and water (volume ratio = 1:1). The whole system is put in a constant temperature oscillator (THZ-320, Shanghai Jinghong

Experimental Equipment Co., Ltd, China). 5 mL outer liquid is withdrawn and detected by UV spectrophotometer (UV-1780, Shimadzu, Japan) because the pyraclostrobin has a characteristic absorption peak at 275 nm, and 5 mL acetonitrile and water (volume ratio = 1:1) are put back, the procedure is repeated every 1 h for 12 h and every 12 h following[19].

3. Results and discussion

3.1. Fabrication of pyraclostrobin-loaded PLGA microcapsules

As mentioned above, the pyraclostrobin-loaded PLGA microcapsules are fabricated by LDCFF process followed by solvent evaporation. Figure 2 shows the details of the microcapsules' formation. Figure 2a shows that the fluids flowing from the coaxial needle formed the stable cone, focused by the focusing fluid and passing through the small orifice. Then the jet breaks up into uniform microdroplets with pyraclostrobin suspension encapsulated by outer shell liquid, as shown in Figure 2b. It should be noted that Figure 2a is reflective image while Figure 2b is transparent image.

3.2. Characterization of pyraclostrobin-loaded PLGA microcapsules

As the pyraclostrobin suspension is opaque, microcapsules are black spheres by optical microscopy observation in Figure 3a. The SEM image Figure 3b shows the surface conditions of the microcapsules which is smooth with little
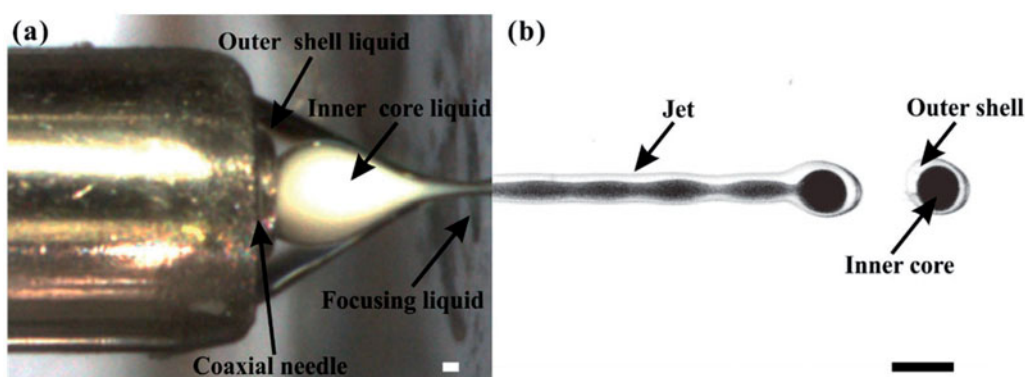

Figure 2. Illustration of the LDCFF process to fabricate PLGA microcapsules: (a) a steady cone-jet mode in the LDCFF process, (b) breakup of the liquid jet (scale bar: 50 μm).
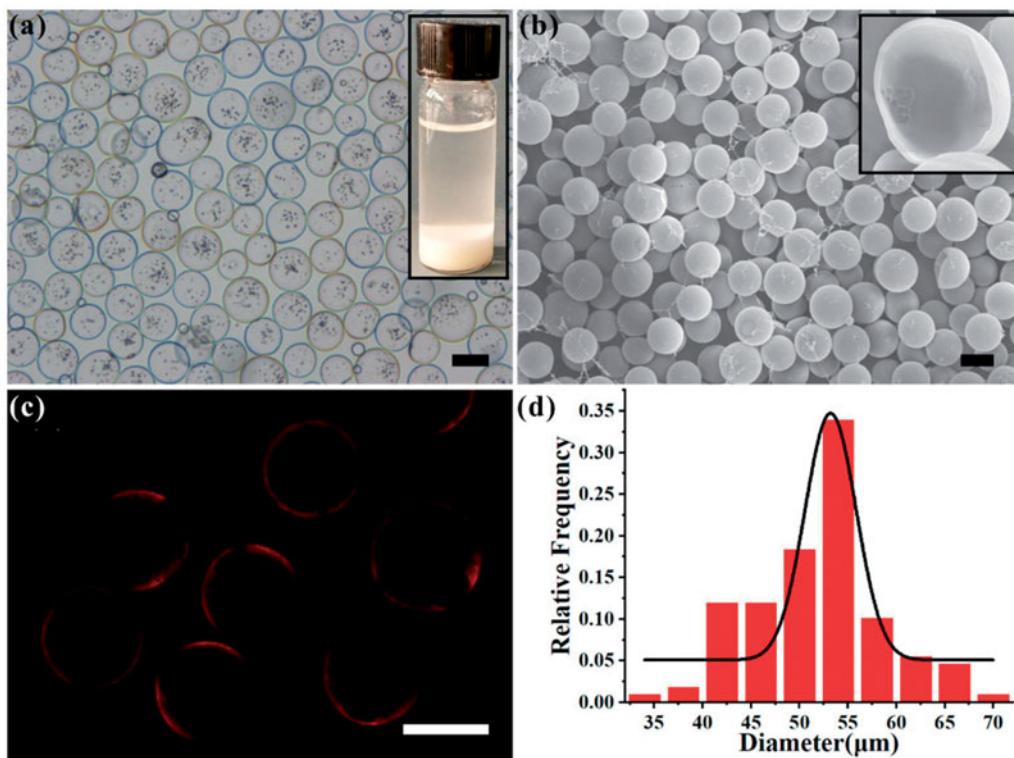

Figure 3. Characteristics of the produced PLGA microcapsules: (a) the microscopy image of morphology, (b) the SEM image of PLGA microcapsules and (c) the confocal fluorescence microscopic image; (d) the size distribution of PLGA microcapsules, the average of diameter is 51.95 μm, PDI = 0.050, the liquid flow rates: $Q_i =$ 5 mL/h, $Q_o =$ 5 mL/h, $Q_f =$ 800 mL/h (scale bar: 50 μm).
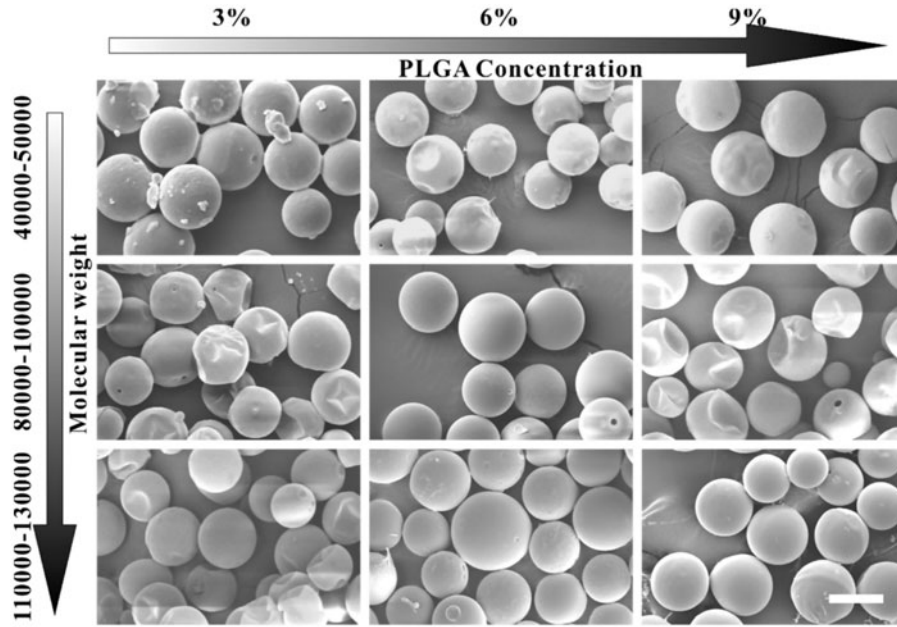
Figure 4. PLGA microcapsules with different molecular weights (40000-50000, 80000-100000 and 1100000-1300000 g/mol) and different concentrations (30, 60 and 90 mg/mL) (scale bar: 50 μm). The liquid flow rates: $Q_i = 5$ mL/h, $Q_o = 5$ mL/h, $Q_f = 800$ mL/h.

porosity, so the pyraclostrobin suspended in water can not escape from the microcapsules. Some methyindocarbocyanine perchlorate is added into the outer shell liquid as fluorescence dye and the confocal fluorescence microscopic image is shown in Figure 3c to prove the microcapsules' core-shell structure. The pyraclostrobin suspension is totally encapsulated by the outer shell liquid. After solvent evaporation, distilled water washing and vacuum freezing drying, the pyraclostrobin-loaded PLGA microcapsules are collected. Those images can also explain why the EE should be 100% in theory for that there is no leakage of pyraclostrobin suspension in LDCFF process. When $Q_i = Q_o = 5$ mL/h, $Q_f = 800$ mL/h, the average diameter of microcapsules is 51.95 μm and PDI is 5.0%, as is shown in Figure 3d. The yield of microcapsules in LDCFF process is about 3.8×10^4 Hz. In addition, the prepared microcapsules with different PLGA molecular weights and concentrations are shown in Figure 4. The results show that microcapsules with good morphology can be obtained in a wide range of parameters.

3.3. Size and shell thickness control of pyraclostrobin-loaded PLGA microcapsules

In our experiment, microcapsules with tens to hundreds microns can be fabricated. The properties of fluids would also influence the size of the microcapsules. Figure 5a–d show the relationships between the diameters of the produced microcapsules and the liquid flow rates of the three phases. It should be noted that the sizes of microcapsules here are measured from the microscopic images of the microcapsules directly collected after the breakup of liquid jets, which would be different from the SEM results shown in Figure 4, as the post-processing for SEM imaging would change the size of microcapsules.

The diameters of microcapsules increase with the increase of Q_i, Q_o and $Q_i + Q_o$ and decrease with the increase of Q_f. The Eq. 4 shows the scaling law:

$$D \sim \alpha \left[(Q_i + Q_o)/Q_f \right]^{1/2} \cdot D_{orif} \qquad (4)$$

where α is a constant depending on the properties of fluids, D, D_{orif} are the diameters of microcapsule and orifice, Q_i, Q_o, Q_f are the flow rates of inner core liquid, outer shell liquid and focusing liquid, respectively. Adjusting Q_i, Q_o and Q_f can achieve the control of the microcapsules' size and shell thickness. When Q_f increases or Q_i and Q_o decrease, the sizes and shell thicknesses of microcapsules decrease.

The stability of the cone-jet configuration under different flow rate ratios of internal and external phases ($\varphi = Q_i/Q_o$) is demonstrated in Figure 6. Microcapsules with different shell thicknesses can also be prepared by adjusting flow rate ratio φ. Figure 6a–c show the experimental images of the stable cone-jet morphology changing with φ (7:3, 5:5, 1:9) when $Q_i + Q_o = 10$ mL/h, $Q_f = 800$ mL/h. As φ decreases, the inner Taylor cone becomes thinner and the shell thickness of the microcapsules becomes thicker. When φ is greater than a certain threshold, the prepared microdroplets only have one core, as shown in Figure 6d,e. However, when φ is less than a certain threshold, the prepared microdroplets will have multiple cores, as shown in Figure 6f. The shell thickness depends on the diameters of microcapsules and the proportion of Q_i, Q_o. Also, the Eq. 5 shows the scaling law when each of the prepared microdroplets has only one core:

$$d \sim \left[1 - Q_i^{1/3}/(Q_i + Q_o)^{1/3} \right] \cdot D \qquad (5)$$

where d is the average shell thickness, D is the diameters of microcapsules, Q_i, Q_o are the flow rates of inner core liquid, outer shell liquid, respectively.
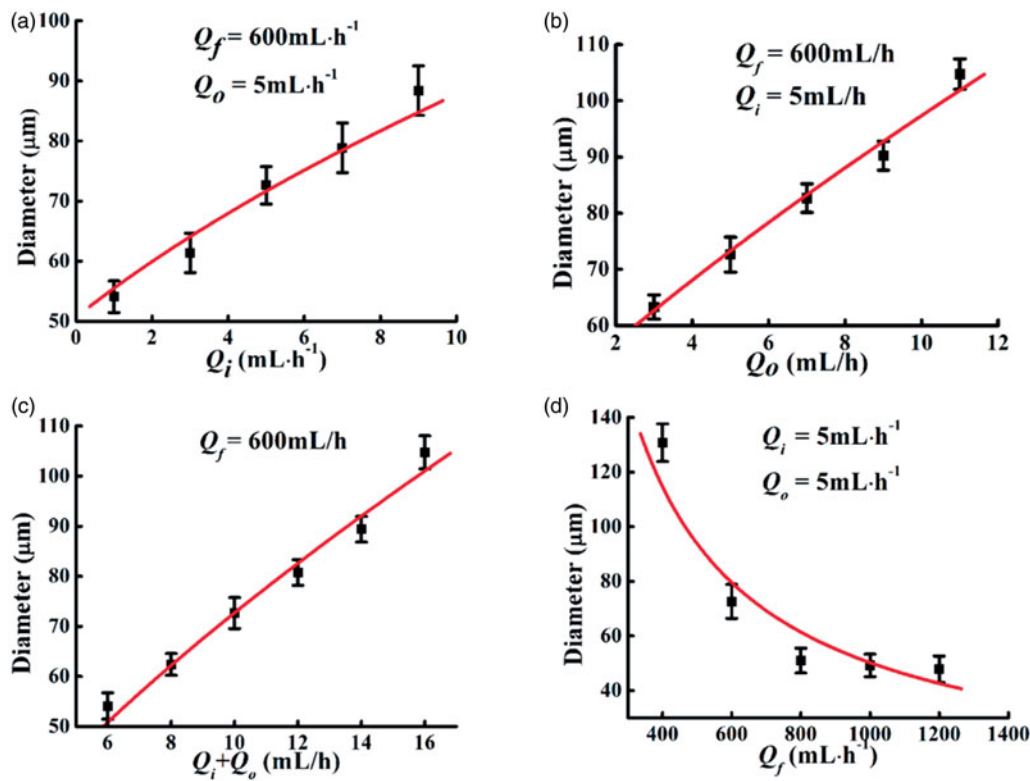
Figure 5. Size control of PLGA microcapsules by changing Q_i, Q_o, Q_f: (a) diameter D changes with Q_i for $Q_f = 600$ mL/h and $Q_o = 5$ mL/h; (b) diameter D changes with of Q_o for $Q_f = 600$ mL/h and $Q_i = 5$ mL/h; (c) diameter D changes with $Q_i + Q_o$ for $Q_f = 600$ mL/h and $Q_o = 5$ mL/h; (d) diameter D changes with Q_f for $Q_i = Q_o = 5$ mL/h.
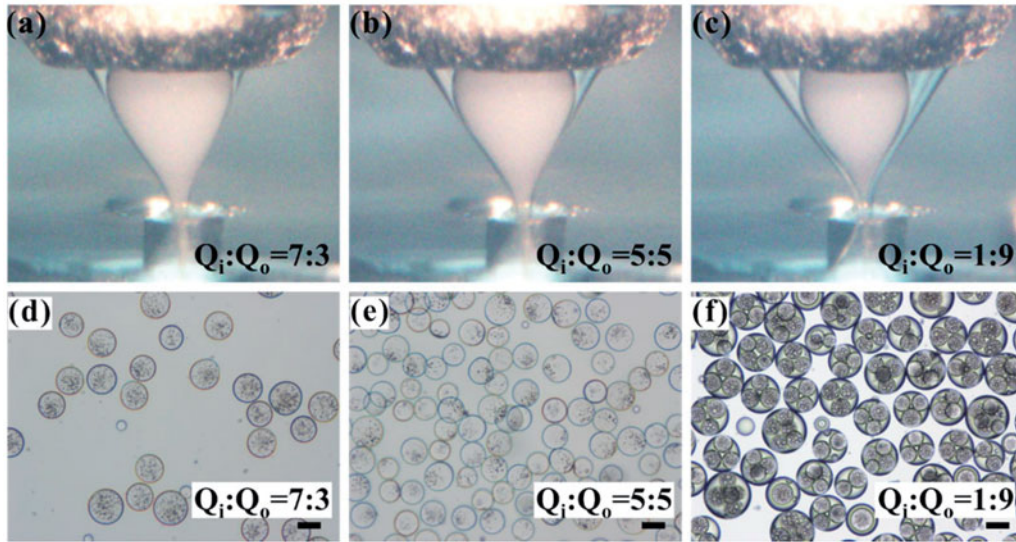

Figure 6. Shell thickness control of PLGA microcapsules by changing flow rate ratios of internal and external phases ($\varphi = Q_i/Q_o$): (a) ∼ (c) sequence of experimental images showing the cone-jet structure changing with φ (7:3, 5:5, 1:9); (d) ∼ (f) the morphologies of the produced microdroplets changing with φ (7:3, 5:5, 1:9). The liquid flow rates: $Q_i + Q_o = 10$ mL/h, $Q_f = 800$ mL/h (scale bar: 50 μm).

3.4. Pyraclostrobin sustained release with different PLGA microcapsules

We choose three typically different kinds of PLGA microcapsules to compare and simulate the pyraclostrobin release, as shown in Figure 7. Sample A is made by $Q_i = 6$ mL/h, $Q_o = 4$ mL/h, $Q_f = 600$ mL/h, sample B is made by $Q_i = 6$ mL/h, $Q_o = 6$ mL/h, $Q_f = 600$ mL/h, sample C is made by $Q_i = 10$ mL/h, $Q_o = 10$ mL/h, $Q_f = 600$ mL/h respectively.

Based on the scaling law, the microcapsules' sizes and shell thicknesses increase from sample A to C. Samples A, B and C show the different effects on pyraclostrobin cumulative release profile. It can be easily seen that the drug release would be faster with smaller size. On one hand, smaller size of microcapsules results in shorter average distance between the encapsulated pyraclostrobin and the surface of microcapsules, so the pyraclostrobin would be easier to diffuse into
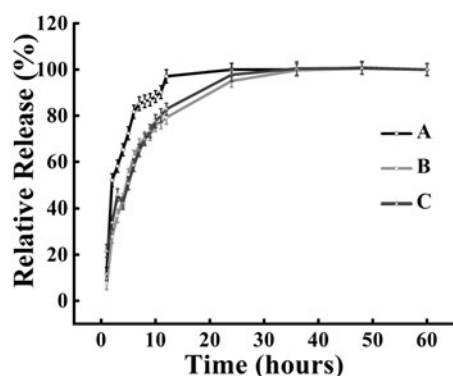
Figure 7. Effect of different microcapsules on pyraclostrobin cumulative release profile. Sample A for $Q_i = 6\,mL/h$, $Q_o = 4\,mL/h$, $Q_f = 600\,mL/h$, sample B for $Q_i = Q_o = 6\,mL/h$, $Q_f = 600\,mL/h$, sample C for $Q_i = Q_o = 10\,mL/h$, $Q_f = 600\,mL/h$.

the external environment of the microcapsules. On the other hand, small microcapsules get bigger specific surface area, which causes the PLGA membrane eruption more easily by the mixed solution. Generally, the mechanisms of drug release from polymer microcapsules include three ways[40]: the drug diffusing through the polymer matrix, diffusing through pores inside polymer matrix (aqueous channels) and liberation in the degradation or erosion process of the polymer matrix. In our experiment, the mixed solution can easily dissolve pyraclostrobin but it can not dissolve PLGA. It could destroy the structure of PLGA membrane, which is also simulated as the degradation and erosion of PLGA in the natural environment (faster than natural degradation). When PLGA is "degraded or eroded", there would be a faster release. Therefore, the "degradation" of PLGA microcapsules may be the possible reason of the shoulders in the profiles.

4. Conclusions

In this work, we have prepared pyraclostrobin-loaded PLGA microcapsules with controlled size, high EE and LE fabricated by the LDCFF process. The influences of the liquid flow rates on the size and shell thickness of the produced microcapsules are investigated. The results indicate that the sizes of microcapsules can be easily controlled by adjusting the main process parameters Q_i, Q_o, Q_f, and D_{orif}. Pyraclostrobin sustained release profiles are further investigated. The results show that the LDCFF process also offers controlled release rates by just changing the diameter and the shell thickness of microcapsules that are closely related to the fluid flow rates and the concentration of wall materials. The LDCFF method also provides a great potential in producing microcapsules with different sizes, structures and material combinations for various applications.

Funding

References

[1] Wang, C.; Wang, F.; Zhang, Q.; Liang, W. Individual and Combined Effects of Tebuconazole and Carbendazim on Soil Microbial Activity. *Eur. J. Soil Biol.* **2016**, *72*, 6–13. doi:10.1016/j.ejsobi.2015.12.005.

[2] Yin, M-m.; Zheng, Y.; Chen, F-l. Pyraclostrobin-loaded poly (lactic-co-glycolic acid) nanospheres: Preparation and characteristics. *J. Integr. Agric.* **2018**, *17*, 1822–1832. doi:10.1016/S2095-3119(17)61839-2.

[3] Meyer, C.; Pieper, C. C.; Ezziddin, S.; Wilhelm, K. E.; Schild, H. H.; Ahmadzadehfar, H. Feasibility of Temporary Protective Embolization of Normal Liver Tissue Using Degradable Starch Microspheres during Radioembolization of Liver Tumours. *Eur. J. Nucl. Med. Mol. Imaging.* **2014**, *41*, 231–237. doi:10.1007/s00259-013-2550-4.

[4] Yongquan, Z. Development and Prospects of the Research on Pesticide Residues. *Plant Prot.* **2013**, *39*, 90–98.

[5] Chevillard, A.; Angellier-Coussy, H.; Guillard, V.; Gontard, N.; Gastaldi, E. Controlling Pesticide Release via Structuring Agropolymer and Nanoclays Based Materials. *J. Hazard. Mater.* **2012**, *205–206*, 32–39. doi:10.1016/j.jhazmat.2011.11.093.

[6] Huang, A.; Huang, Z.; Dong, Y.; Chen, L.; Fu, L.; Li, L.; Ma, L. Controlled Release of Phoxim from Organobentonite Based Formulation. *Appl. Clay Sci.* **2013**, *80–81*, 63–68. doi:10.1016/j.clay.2013.06.010.

[7] Zeinali, M.; McConnell, L. L.; Hapeman, C. J.; Nguyen, A.; Schmidt, W. F.; Howard, C. J. Volatile Organic Compounds in Pesticide Formulations: Methods to Estimate Ozone Formation Potential. *Atmos. Environ.* **2011**, *45*, 2404–2412. doi:10.1016/j.atmosenv.2011.02.015.

[8] Meredith, A. N.; Harper, B.; Harper, S. L. The Influence of Size on the Toxicity of an Encapsulated Pesticide: A Comparison of Micron- and Nano-Sized Capsules. *Environ. Int.* **2016**, *86*, 68–74. doi:10.1016/j.envint.2015.10.012.

[9] Kobašlija, M.; McQuade, D. T. Polyurea Microcapsules from Oil-in-Oil Emulsions via Interfacial Polymerization. *Macromolecules* **2006**, *39*, 6371–6375. doi:10.1021/ma061455x.

[10] Tsuda, N.; Ohtsubo, T.; Fuji, M. Preparation of Self-Bursting Microcapsules by Interfacial Polymerization. *Adv. Powder. Technol.* **2012**, *23*, 724–730. doi:10.1016/j.apt.2011.09.005.

[11] Yuan, H.; Li, G.; Yang, L.; Yan, X.; Yang, D. Development of Melamine-Formaldehyde Resin Microcapsules with Low Formaldehyde Emission Suited for Seed Treatment. *Colloids Surf B Biointerfaces* **2015**, *128*, 149–154. doi: 10.1016/j.colsurfb.2015.02.029.

[12] Rojas-Moreno, S.; Osorio-Revilla, G.; Gallardo-Velazquez, T.; Cardenas-Bailon, F.; Meza-Marquez, G. Effect of the Cross-Linking Agent and Drying Method on Encapsulation Efficiency of Orange Essential Oil by Complex Coacervation Using Whey Protein Isolate with Different Polysaccharides. *J. Microencapsul.* **2018**, *35*, 1–16. doi:10.1080/02652048.2018.1449910.

[13] Butstraen, C.; Salaun, F. Preparation of Microcapsules by Complex Coacervation of Gum Arabic and Chitosan. *Carbohydr. Polym.* **2014**, *99*, 608–616. doi: 10.1016/j.carbpol.2013.09.006.

[14] Dai, R. Y.; You, S. Y.; Lu, L. M.; Liu, Q.; Li, Z. X.; Wei, L.; Huang, X. G.; Yang, Z. Y. High Blades Spreadability of Chlorpyrifos Microcapsules Prepared with Polysiloxane Sodium Carboxylate/Sodium Carboxymethylcellulose/Gelatin via Complex Coacervation. *Colloids Surf. A Physicochem. Eng. Asp.* **2017**, *530*, 13–19. doi:10.1016/j.colsurfa.2017.06.057.

[15] Yang, N.; Shen, K.; Guo, J.; Tao, X.; Xu, P.; Mao, H. Error Analysis for Pesticide Detection Performed on Paper-Based Microfluidic Chip Devices. *Mod. Phys. Lett. B* **2017**, *31*, 1740024. doi:10.1142/S0217984917400243.

[16] Lin, Y.-S.; Liu, J. In CD-like centrifugal microfluidic device for organophosphorus pesticides (OPP) sensing. Presented at the International Conference on Optical MEMS and Nanophotonics (OMN), Santa Fe, NM, Aug 13–17, 2017.

[17] Liu, J.; Lan, Y.; Yu, Z.; Tan, C. S.; Parker, R. M.; Abell, C.; Scherman, O. A. Cucurbit[n]uril-Based Microcapsules Self-Assembled within Microfluidic Droplets: A Versatile Approach for Supramolecular Architectures and Materials. *Acc. Chem. Res.* **2017**, *50*, 208–217. doi:10.1021/acs.accounts.6b00429.

[18] Nangrejo, M.; Ahmad, Z.; Edirisinghe, M. Ceramic Encapsulation with Polymer via co-Axial Electrohydrodynamic Jetting. *J. Microencapsul.* **2010**, *27*, 542–551. doi:10.3109/02652048.2010.489973.

[19] Yuan, S.; Lei, F.; Liu, Z.; Tong, Q.; Si, T.; Xu, R. X. Coaxial Electrospray of Curcumin-Loaded Microparticles for Sustained Drug Release. *PLoS One* **2015**, *10*, e0132609. doi:10.1371/journal.pone.0132609.

[20] Jaworek, A. Electrostatic Micro- and Nanoencapsulation and Electroemulsification: A Brief Review. *J. Microencapsul.* **2008**, *25*, 443–468. doi:10.1080/02652040802049109.

[21] Vladisavljević, G. T.; Khalid, N.; Neves, M. A.; Kuroiwa, T.; Nakajima, M.; Uemura, K.; Ichikawa, S.; Kobayashi, I. Industrial Lab-on-a-Chip: design, Applications and Scale-up for Drug Discovery and Delivery. *Adv. Drug Deliv. Rev.* **2013**, *65*, 1626–1663. doi:10.1016/j.addr.2013.07.017.

[22] Kong, F.; Zhang, X.; Hai, M. Microfluidics Fabrication of Monodisperse Biocompatible Phospholipid Vesicles for Encapsulation and Delivery of Hydrophilic Drug or Active Compound. *Langmuir.* **2014**, *30*, 3905–3912. doi:10.1021/la404201m.

[23] Bardin, D.; Martz, T. D.; Sheeran, P. S.; Shih, R.; Dayton, P. A.; Lee, A. P. High-Speed, Clinical-Scale Microfluidic Generation of Stable Phase-Change Droplets for Gas Embolotherapy. *Lab. Chip.* **2011**, *11*, 3990–3998. doi:10.1039/c1lc20615j.

[24] Bardin, D.; Kendall, M. R.; Dayton, P. A.; Lee, A. P. Parallel Generation of Uniform Fine Droplets at Hundreds of Kilohertz in a Flow-Focusing Module. *Biomicrofluidics* **2013**, *7*, 34112. doi:10.1063/1.4811276.

[25] Zhu, Z.; Wu, Q.; Han, S.; Xu, W.; Zhong, F.; Yuan, S.; Dwivedi, P.; Si, T.; Xu, R. X. Rapid Production of Single- and Multi-Compartment Polymeric Microcapsules in a Facile 3D Microfluidic Process for Magnetic Separation and Synergistic Delivery. *Sens. Actuators B Chem.* **2018**, *275*, 190–198. doi: 10.1016/j.snb.2018.08.044.

[26] Wu, Q.; Yang, C. Y.; Yang, J. X.; Huang, F. S.; Liu, G. L.; Zhu, Z. Q.; Si, T.; Xu, R. X. Photopolymerization of Complex Emulsions with Irregular Shapes Fabricated by Multiplex Coaxial Flow Focusing. *Appl. Phys. Lett.* **2018**, *112*, 071601. doi:10.1063/1.5018207.

[27] Cozar-Bernal, M. J.; Holgado, M. A.; Arias, J. L.; Munoz-Rubio, I.; Martin-Banderas, L.; Alvarez-Fuentes, J.; Fernandez-Arevalo, M. Insulin-Loaded PLGA Microparticles: flow Focusing versus Double Emulsion/Solvent Evaporation. *J. Microencapsul.* **2011**, *28*, 430–441. doi:10.3109/02652048.2011.576786.

[28] Zhu, Z.; Si, T.; Xu, R. X. Microencapsulation of Indocyanine Green for Potential Applications in image-guided drug delivery. *Lab. Chip.* **2015**, *15*, 646–649. doi:10.1039/c4lc01032a.

[29] Gavini, E.; Mariani, A.; Rassu, G.; Bidali, S.; Spada, G.; Bonferoni, M. C.; Giunchedi, P. Frontal Polymerization as a New Method for Developing Drug Controlled Release Systems (DCRS) Based on Polyacrylamide. *Eur. Polym. J.* **2009**, *45*, 690–699. doi:10.1016/j.eurpolymj.2008.12.017.

[30] Mirabedini, S. M.; Dutil, I.; Farnood, R. R. Preparation and Characterization of Ethyl Cellulose-Based Core–Shell Microcapsules Containing Plant Oils. *Colloids. Surf. A Physicochem. Eng. Asp.* **2012**, *394*, 74–84. doi:10.1016/j.colsurfa.2011.11.028.

[31] Li, D.; Liu, B.; Yang, F.; Wang, X.; Shen, H.; Wu, D. Preparation of Uniform Starch Microcapsules by Premix Membrane Emulsion for Controlled Release of Avermectin. *Carbohydr. Polym.* **2016**, *136*, 341–349. doi:10.1016/j.carbpol.2015.09.050.

[32] Xu, C.; Cao, L.; Zhao, P.; Zhou, Z.; Cao, C.; Zhu, F.; Li, F.; Huang, Q. Synthesis and Characterization of Stimuli-Responsive Poly(2-Dimethylamino-Ethylmethacrylate)-Grafted Chitosan Microcapsule for Controlled Pyraclostrobin Release. *Int. J. Mol. Sci.* **2018**, *19*, E854. doi:10.3390/ijms19030854.

[33] Makadia, H. K.; Siegel, S. J. Poly Lactic-co-Glycolic Acid (PLGA) as Biodegradable Controlled Drug Delivery Carrier. *Polymers* **2011**, *3*, 1377–1397. doi:10.3390/polym3031377.

[34] Si, T.; Feng, H.; Luo, X.; Xu, R. X. Formation of Steady Compound Cone-Jet Modes and Multilayered Droplets in a Tri-Axial Capillary Flow Focusing Device. *Microfluid. Nanofluid.* **2015**, *18*, 967–977. doi:10.1007/s10404-014-1486-8.

[35] Wu, Q.; Yang, C.; Liu, G.; Xu, W.; Zhu, Z.; Si, T.; Xu, R. X. Multiplex Coaxial Flow Focusing for Producing Multicompartment Janus Microcapsules with Tunable Material Compositions and Structural Characteristics. *Lab. Chip.* **2017**, *17*, 3168–3175. doi:10.1039/C7LC00769H.

[36] Si, T.; Li, F.; Yin, X.-Y.; Yin, X.-Z. Modes in Flow Focusing and Instability of Coaxial Liquid–Gas Jets. *J. Fluid Mech.* **2009**, *629*, 1–23. doi:10.1017/S0022112009006211.

[37] Li, G.; Luo, X.; Si, T.; Xu, R. X. Temporal Instability of Coflowing Liquid-Gas Jets under an Electric Field. *Phys. Fluids.* **2014**, *26*, 054101. doi:10.1063/1.4875109.

[38] Loscertales, I. G.; Barrero, A.; Guerrero, I.; Cortijo, R.; Marquez, M.; Ganan-Calvo, A. Micro/Nano Encapsulation via Electrified Coaxial Liquid Jets. *Science* **2002**, *295*, 1695–1698. doi:10.1126/science.1067595.

[39] Kaufman, J. J.; Tao, G.; Shabahang, S.; Banaei, E.-H.; Deng, D. S.; Liang, X.; Johnson, S. G.; Fink, Y.; Abouraddy, A. F. Structured Spheres Generated by an in-Fibre Fluid Instability. *Nature* **2012**, *487*, 463. doi:10.1038/nature11215.

[40] Athanasiou, K. A.; Niederauer, G. G.; Agrawal, C. M. Sterilization, Toxicity, Biocompatibility and Clinical Applications of Polylactic Acid/Polyglycolic Acid Copolymers. *Biomaterials* **1996**, *17*, 93–102. doi:10.1016/0142-9612(96)85754-1.